Quantitative Analysis of Damage in PBX 9501 Subjected to a Linear Thermal Gradient

Blaine Asay, Bryan Henson, Paul Peterson,
Joseph Mang, Laura Smilowitz, and Peter Dickson
Los Alamos National Laboratory, Los Alamos, NM

We have conducted a series of experiments in which a cylinder of PBX 9501 is placed in a specially designed fixture with, each end fixed at a different temperature. This arrangement sets up a thermal gradient in the explosive that is carefully controlled and maintained for a specified amount of time. This configuration has a number of advantages over thermally damaging separate pieces at a series of different temperatures, the principal one being that damage in this experiment is a continuous function of position. This makes analysis and distinction of regions easier and more straightforward. For the experiments reported in this paper, the explosive samples have been subjected to a series of different analysis techniques. We have used polarized light microscopy, physical adsorption, Raman spectroscopy, and small angle neutron and x-ray scattering in an attempt to characterize the particle morphology, porosity distribution, crack and void formation, and chemical state as a function of thermal treatment. While not all of the efforts were informative, the data clearly show trends and form a basis for understanding the effects of thermal damage on explosive behavior.

INTRODUCTION

Damaged explosives behave much differently than pristine materials when subjected to thermal or mechanical stimuli, and they are considered to be more sensitive in general. However, the type of damage that each treatment creates is different. Thermally induced damage is both chemical and physical in nature. For example in HMX, once the temperature has exceeded the beta-delta phase transition temperature (~159 C), chemical change controlled by Arrhenius kinetics begins to evolve both solid and gaseous decomposition products. These serve to modify the response of the explosive to any further stimuli. The phase transition also effects a large change (~7%) in the density and crystal morphology. This necessarily creates many voids and other defects at the crystalline level that form potential hot spots for shock initiation as well as increased surface area for enhanced combustion. All of these modifications change the material's properties and equation of state. Damage from a mechanical source does not necessarily cause chemical changes, but if high temperatures are the result of shear bands or other stress localization, such changes can occur.

The role of damage in increased violence of reactions has been suggested but not fully demonstrated. It is known that in some cases, preheated explosive ignites more readily than untreated material, and that damaged explosive can

be more sensitive to shock. However, no general conclusions can be drawn, in part because the notion of how to define damage has not been well established. For example, while damage may result in inclusions and other defects, if they are sufficiently small then they will not be effective hot spots for shock initiation.

We have conducted an experiment in which we subjected a sample of PBX 9501 to a well-defined thermal profile that resulted in damage. We then analyzed the sample using several techniques in an attempt to correlate the damage that occurred and develop a more quantitative definition. The linear damage procedure will first be described. Then the results from each technique will be presented. Finally the data will be summarized.

EXPERIMENTAL

Figure 1 shows the configuration for the experiment. It consists of a 6- x 76-mm cylinder of PBX 9501 encased in a copper case and secured at each end with copper endplates. No attempt was made to hermitically seal the explosive. For the first experiment, both endplates were heated. However for the last two, only one endplate was in contact with a foil heater in order to maximize the thermal gradient. Experiment 1 thus had a more shallow gradient, and the time taken to reach equilibrium was longer as well. Current was supplied by a variac and the temperature was controlled manually. The explosive with the confinement was placed inside a threaded plastic cage into which the end caps were affixed. Thermocouples were placed on the outside of the case.

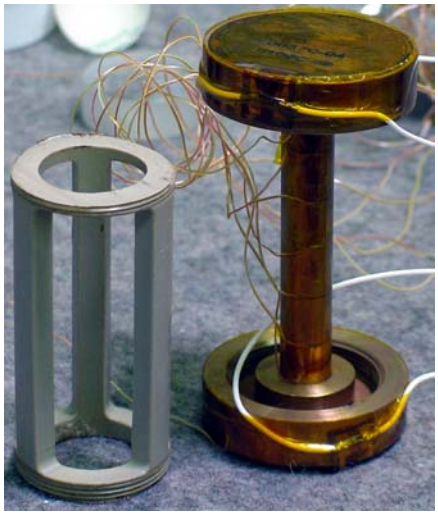

FIGURE. 1. Photograph OF LINEAR DAMAGE EXPERIMENT

Once assembled, the entire assembly was wrapped in glass wool. The sample was first heated quickly so that it was everywhere above the phase transition temperature. The temperature was then raised more slowly until the desired profile was achieved. Figures 2-4 show the temperature history for experiment 1-3 respectively. The positions shown on figure 2 for each of the temperature traces are the same as for the other experiments. Note that the total time for experiment 1 is much longer than for the other experiments.

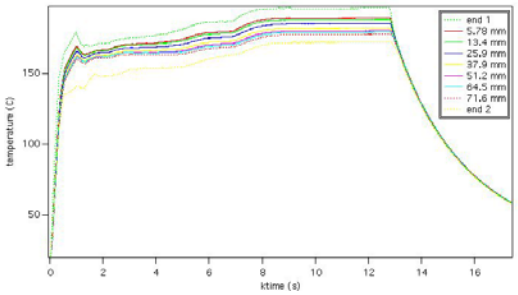

FIGURE 2. TEMPERATURE HISTORY FOR EXPERIMENT 1.

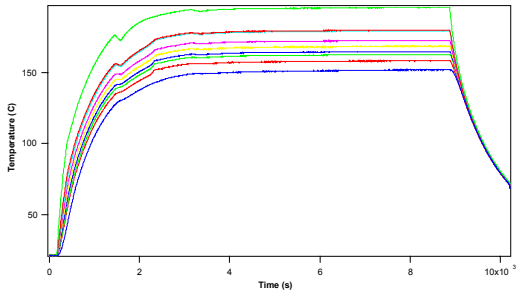

FIGURE 3. TEMPERATURE HISTORY FOR EXPERIMENT 2.

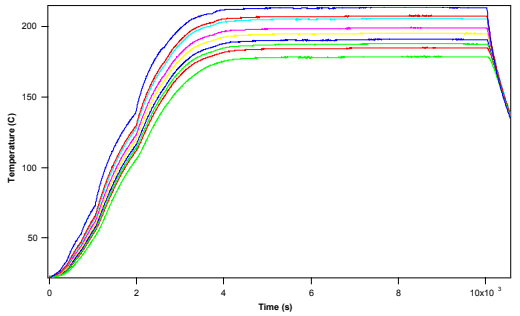

FIGURE 4. TEMPERATURE HISTORY FOR EXPERIMENT 3

Constant temperatures were held for approx. 6500 s.

Figure 5 shows a compilation of the thermal gradients from each of the experiments during the steady portion of the experiment. The highest and lowest temperatures are those at the end caps. They then change monotonically along the sample. Even though the temperatures for experiment 1 were nominally between those of the other two experiments, the total experimental soak time was much longer. To obtain a continuous temperature profile for each sample, a line was fit to the explosive's temperatures. Samples were cut into 4 sections for expt. 1 and 2, and into 5 sections for expt. 3. Average temperatures for each section were calculated by dividing the endpoint values by 2.

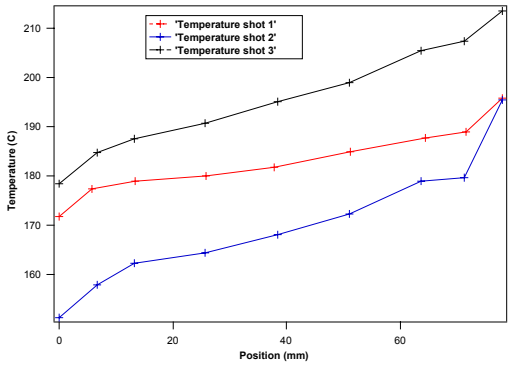

FIGURE 5. TEMPERATURE PROFILES DURING STEADY PORTION OF EXPERIMENT.

Because of the damage and thermal softening, it was difficult to remove the sample without damaging it further, and two of the samples cracked during the operation.

SMALL ANGLE X-RAY SCATTERING

Small angle neutron (SANS) and x-ray scattering (SAXS) measurements were performed at LANL and the University of New Mexico's SAXS Laboratory respectively. The SAXS data were acquired with the Bonse-Hart instrument, [1] which can provide detailed structural information over length scales between 40-10000 Å. SANS was performed on a single sample and the data agree well with the SAXS results, and will not be further described here. In a SAXS experiment, X-rays will scatter from fluctuations in the scattering length density, $\rho(r)$, which reflects microscale structure. The intensity of the scattered radiation, I(Q), is measured as a function of the scattering vector, Q, of magnitude $Q = (4\pi/\lambda) \sin(\theta)$, where λ is the wavelength of the incident radiation and θ is half of the scattering angle. The scattering signal I (Q), for a polydisperse system of non-interacting

particles, dispersed in a uniform media, can be expressed as[2,3]

$$I(Q) = N_v \Delta\rho^2 \int_0^\infty N(R)V(R)^2 \langle P(\mathbf{Q},R)\rangle dR \; w$$

here P (Q,R) is the normalized, single particle form factor and is related to the Fourier transform of ρ(r), V is the particle volume, and N_v is the average particle number density. Δρ is the scattering length density contrast between the average scattering length density of the particle and the surrounding media.

Analysis of the scattering from the PBX 9501 system is complicated because of the different phases present: HMX, binder, and voids. Since HMX accounts for ~ 90% of the volume, it is considered as the continuous phase. The scattering thus arises from the HMX-binder, HMX-void and binder-void interfaces, not from voids within the crystals. With the current data, we cannot distinguish among the three contributions to the scattering signal. However it is possible to measure the total surface area and to obtain size distributions that represent the average size of the binder/void (pore) regions, not including the intergranular defects. The beam width was 1 mm, and measurements were made in the center of the sections described in the introduction.

Figure 6 shows a log-log plot of the scattered x-ray intensity as a function of Q at three representative points (temperatures) along the linear damaged samples. As indicated by the arrows in the figure, deflections or "knees" in the data can be seen, which arise from scattering from distinct populations of pores. The position of the "knee" is indicative of the average size of a pore. From the figure we see that at 159 C, a single population of pores is present over the length scales probed. With increasing temperature, a second population of smaller pores develops, indicating thermally induced changes to the microstructure. In order to quantify these features, the data were fit to a model, assuming lognormal distributions of spherical pores. The results are shown as solid lines in figure 6.

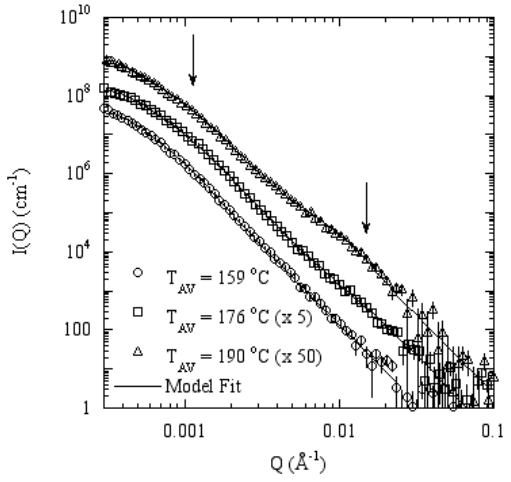

FIGURE 6: SAXS MEASUREMENTS AT THREE TEMPERATURES ALONG THE LINEAR DAMAGED SAMPLES.

Figure 7 displays the volume-weighted pore size distributions extracted from the analysis. From the figure, we see that at the lowest temperature, the data are characterized by the presence of a single distribution of pores centered at R_o ~ 2600 Å (0.26 μm). At T = 176 C, a distribution of smaller pores (R_o ~ 107 Å) develops. With further increase of T, this population nearly doubles in size and is centered at R_o ~ 210 Å at T = 190 C. Similar analysis was performed at different points along the linear damaged samples.

A plot of the number-averaged, mean pore size is shown in figure 8. As we can see from the figure, at lower temperatures the average pore size is approximately constant. At T of approximately 176 C however, we see a large decrease in the average pore size, corresponding to the

development of the new distribution of pores (Fig.7). With increasing T, the average pore size increases monotonically.

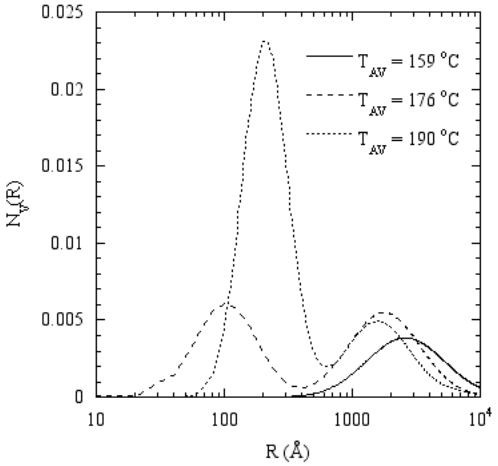

FIGURE 7: PORE SIZE DISTRIBUTIONS DETERMINED BY ANALYSIS OF THE SAXS DATA.

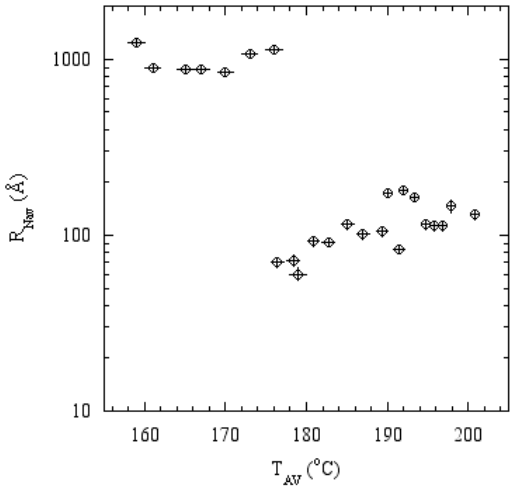

FIGURE 8: NUMBER-AVERAGED MEAN PORE SIZE AS A FUNCTION OF TEMPERATURE FROM SAXS ANALYSIS.

Figure 9 shows a plot of the change in the number density of pores (N_v), with increasing temperature, relative to the number density measured at the lowest temperature (N_{vo}), over the length scales probed. Comparing these data to figure 8, we see that with increasing T (above 176 C), the pores become larger and are fewer in number. We again see the sharp change in N_v at T = 176 C.

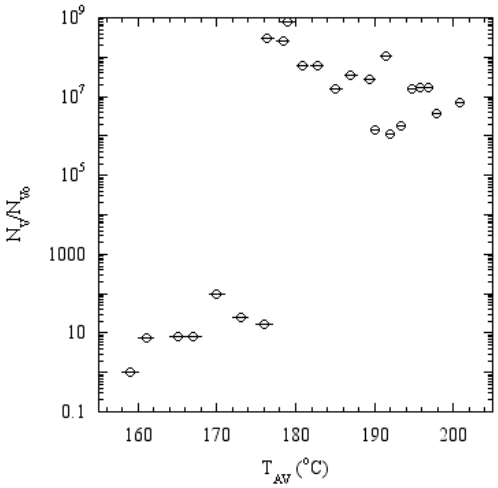

FIGURE 9: AVERAGE NUMBER DENSITY OF PORES AS A FUNCTION OF TEMPERATURE

Analysis of the slope of the high-Q SAXS data allows a measurement of the total surface area[2,3] of the thermally damaged samples. Figure 10 displays the ratio of the surface area per unit volume (S_v) as a function of T, to S_v measured at the lowest temperature (S_o).

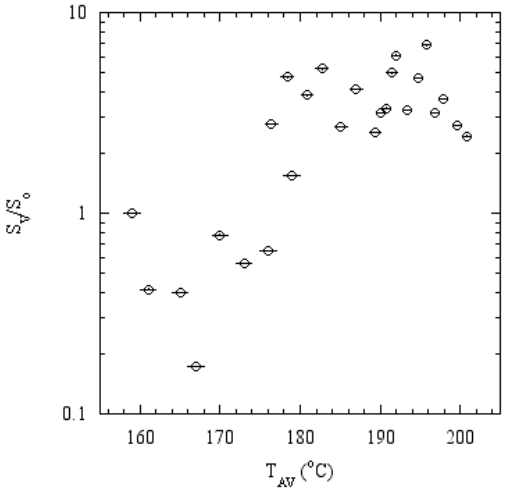

FIGURE 10: TOTAL SURFACE AREA AS A FUNCTION OF TEMPERATURE,

From the figure we see that with increasing temperature there is an increase of surface area, which suggests thermally induced crack and pore development.

PHYSICAL ABSORPTION

These measurements were made in a commercially available instrument (Micromeritics 2400). The experiment consists of quantitatively introducing krypton gas over a known amount of the sample. If the temperature of the sample and pressure of the gas are close to the condensation point of the gas, some amount will adsorb to the sample surface. Known amounts of gas are introduced over samples within calibrated volumes. Absorption lowers the pressure above the sample, and the resulting pressure difference is the amount of gas adsorbed to the surface.

As the pressure is increased up to the condensation pressure, successively more gas is taken up proportional to the surface area. The adsorption isotherm typically used to deduce the surface area from such data is that determined originally by Brunnaer, Emmett and Teller (BET).[4] In BET theory the adsorption of gas is related to the surface area of the sample through

$$\frac{n}{n_m} = \frac{1}{1-x}\frac{cx}{1-x+cx} \qquad (1)$$

where n is the amount of gas taken up and n_m is the amount of gas in a monolayer. The constant ln(c) is proportional to the adsorption free energy and x is the reduced pressure, P/Po, where Po is the condensation pressure. Because of signal-to-noise requirements, it was necessary to use an entire section of the sample. Thus the BET data were more heavily averaged than the SAXS data.

Figure 11 shows the data from all three experiments as a function of average temperature. Samples from experiment 1 were tested twice. The error bars on the lines are calculated from an analysis of the experiment. The fact that the two measurements made on experiment 1 do not overlap within the error bars means that either the treatment between measurements (i.e., the drying and evacuation) was not the same, or the absolute errors were underestimated. However, the gap between the bars is very small.

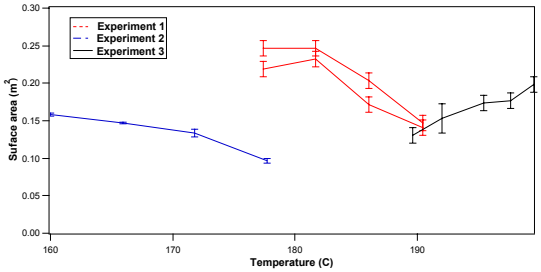

FIGURE 11. SURFACE AREA AS A FUNCTION OF TEMPERATURE

POLARIZED LIGHT MICROSCOPY

Each of the linear damage samples was examined using polarized light microscopy (PLM). To eliminate edge effects, each sample was cut along its centerline, potted in epoxy, and polished as described elsewhere.[5] A total of 36 images were taken at a magnification of 50X along the length of each sample using a Lieca DM-RXA polarizing light microscope and Diagnostic Instruments SPOT 100 CCD camera (1315 x 1033 pixels). Clemex Vision image analysis software was used to determine differences in crystal percentage and average crystal size as a function of

position along the sample, based on image contrast. At this magnification, crystals larger than 3.3μm^2 in size can be differentiated using the analysis routines. We were able to account for nearly 100% of the HMX grains in a pristine sample using this technique.

Results of the analysis are shown in Figure 12. The dotted lines indicate the locations where the samples were sectioned as part of the PLM preparation. The results show a rapid increase in both the overall crystal percentage within the material and the average crystal size between 163 C and 175 C. Further statistical analyses of the images indicates that this is due to an 80% drop in the number of crystals 3.3 μm^2-1000 μm^2 in size. Simultaneously, there is a 12% increase in the number of crystals larger than 1000 μm^2 across the same region. These results suggest that the fine crystals may be dissolving into the nitro-plasticizer and then recrystallizing as part of the larger crystals in this temperature range. Growth of the larger crystals will also result from the phase change across this temperature region.

Between 175.9 C and 194.7 C, both the overall percentage of crystals in the material and the average crystal size decrease. Across this region there is 562% increase in the number of crystals 3.3μm^2-1000μm^2 in size and a 10% decrease in the number of crystals larger than 1000μm^2.

RAMAN SPECTROSCOPY

We placed the linear damage samples in a Raman spectrometer before and after heating. Reasonable spectra were obtained for the undamaged material, but once they were heated, the signal to noise ratio was drastically diminished because of the fluorescence background. We suspect that this arises from decomposition products in the plasticized binder. No satisfactory method was applied to mitigate the problem and thus no data using this technique are reported.

DISCUSSION

The three techniques that were successful each address a different part of the problem. SAXS measures total surface area and defect size, but only that which occurs between grains. Methods such as contrast variation can overcome this limitation, but it was not used on these samples. Also, defect sizes measured are limited to a specified range. The analysis is dependent upon models with several governing assumptions, such as shape of the distribution and pores. BET measures total surface area irrespective of the length scale, but only that which is accessible to gas from outside the sample. A highly porous system, if the pores are not interconnected, would appear to have very low surface area. PLM is limited to observations of a polished surface which by definition is a two dimensional view of a complicated microstructure. Contrast is the only measurable quantity, and inferences must often be made from minor variations in this parameter. A report of these experiments in this forum is of necessity only a survey of what was discovered using several complicated techniques.

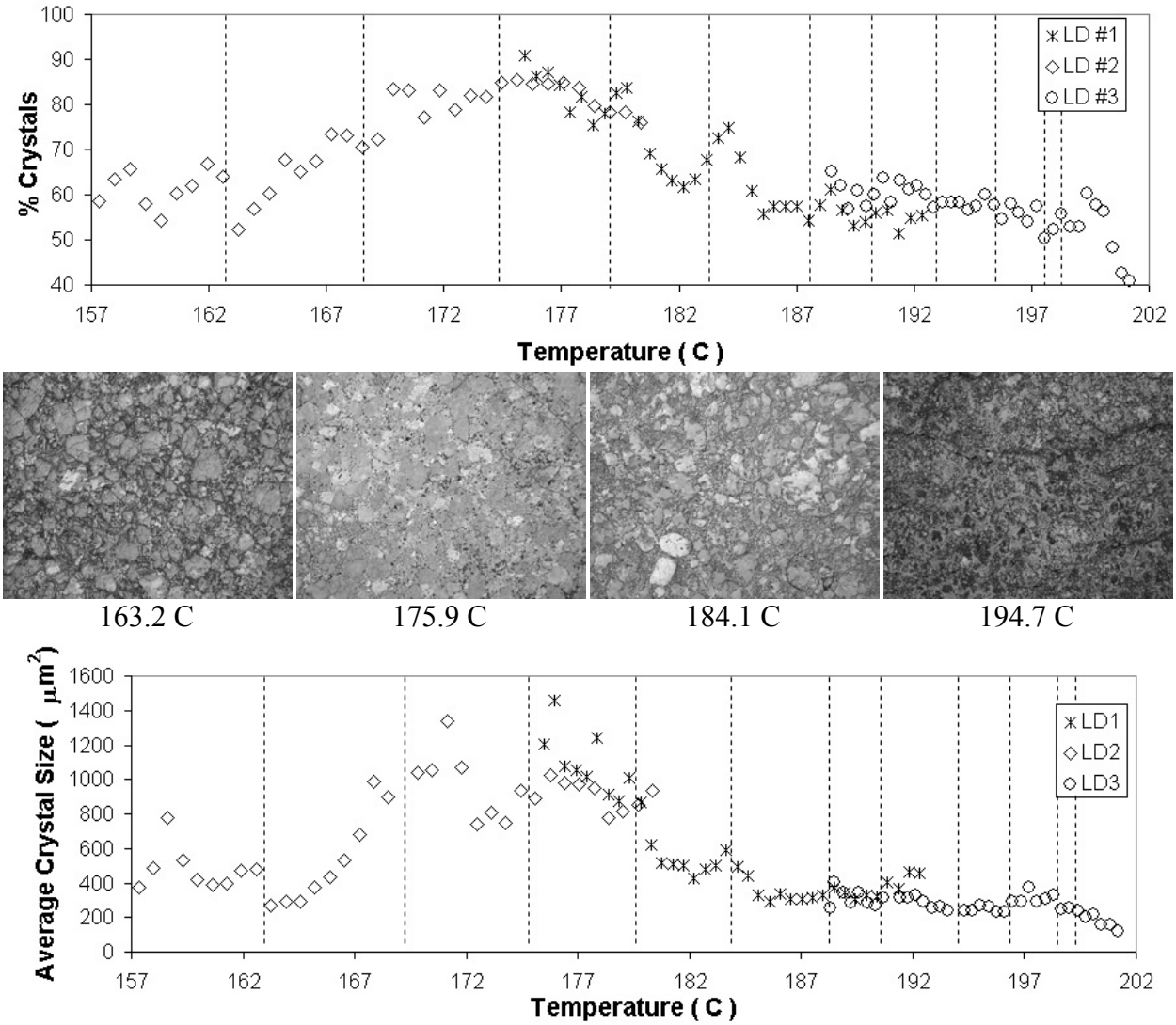

FIGURE 12. RESULTS OF POLARIZED LIGHT MICROSCOPY.

While SAXS and BET measure different variables, they both show remarkably similar trends. SAXS demonstrates an obvious discontinuity in average pore size, number density of pores and surface area per unit volume at ~176 C. A critical observation is that this discontinuity occurred in a single section of the sample from experiment 2, not between sections (which might lead to questions as to whether it is a real effect or an artifact). BET shows precisely the same behavior, but unfortunately this method required averaging over a larger sample size so the break occurs across samples, not within a section. The phase transition occurs at approximately 160 C for slow heating, 15-20 degrees lower than this jump in area measured by SAXS and BET. The temperature will be higher for faster ramp rates. The surface area values are relatively constant in the temperature region where a large increase might be expected. However the pore size distribution changes

dramatically through this region. This is important because for some mechanisms, defect size distribution will dominate initiation (e.g., hot spots for shocks) while surface area is important in others (e.g., combustion).

The surface area trends at higher temperatures are different for SAXS and BET, with SAXS showing slowly rising values and BET showing a minimum at ~190 C. Because BET is very sensitive to binder migration and subsequent pore closure, this might be a more difficult result to analyze quantitatively, but once again, the points from one end of experiment 3 and the other end of experiment 1 overlap. Thus it is evident that while complicated, the results are consistent.

PLM shows that particle size increases during and immediately after the phase change, but then decreases as the rate of gas and solid phase reactions begins to increase. Complicated solution chemistry is also at play as HMX is soluble in the plasticized estane. At the interface between particles and binder, it is known that phase transition is nucleated, and thus, because of the solution chemistry, particle size will play an important role. It is possible that decomposition chemistry is also modified in that region.

The results from all three techniques are remarkably consistent, even though they come from three different samples that were heated using different profiles, and soaked for different amounts of time. The measurements taken at the ends of each sample nicely overlay with each other for all three techniques for experiments 2 and 3, and for SAXS and PLM in experiment 1 (BET may very well overlay for experiment 1, but it is not apparent because of the averaging discussed earlier). PLM demonstrates the continuity particularly well, with multiple independent measurements on each sample. Thus there is continuity between total intraparticle surface area, total accessible surface area, and crystal size from sample to sample. We believe that this constitutes an important result of this work.

CONCLUSIONS

A set of experiments was conducted in which a linear thermal gradient was applied to PBX 9501. Three different techniques were used to characterize the change in material properties as a function of temperature. This data set provides an important initial step in the effort to quantify damage in the future.

REFERENCES

1. Rieker, T. P., Hubbard, P. F., Review of Scientific Instruments, 69, 3504 (1998).

2. Glatter, O. and Kratky, O., Small Angle X-ray Scattering (Academic Press, London, 1982).

3. Mang, J.T., Skidmore C.B., Hjelm R.P., and Howe, P.M., J. Mater. Res., 15, 1199 (2000).

4. A. W. Adamson, The Physical Chemistry of Surfaces (Wiley, New York, 1990).

5. Peterson, P. D., J. T. Mang, S. F. Son, B. W. Asay, M. F. Fletcher, R. P. Hjelm, and E. L. Roemer, “Microstructural Characterization of Energetic Materials”,

Proceedings of the 29th International Pyrotechnics Seminar, Westminster, Colorado, July 14-19, 2002.